Bioorganic & Medicinal Chemistry Letters 21 (2011) 1991–1996

Contents lists available at ScienceDirect

Bioorganic & Medicinal Chemistry Letters

journal homepage: www.elsevier.com/locate/bmcl

Discovery of 3-aryl-5-acylpiperazinyl-pyrazoles as antagonists to the NK_3 receptor

Hamid R. Hoveyda [a,*], Marie-Odile Roy [a], Sebastien Blanc [a], Sophie Noël [a], Joseph M. Salvino [b], Mark A. Ator [b], Graeme Fraser [a]

[a] Euroscreen SA, 47, rue Adrienne Bolland, Gosselies, Belgium
[b] Cephalon Inc., Worldwide Discovery Research, 145 Brandywine Parkway, West Chester, PA 19380, USA

ARTICLE INFO

Article history:
Received 25 December 2010
Revised 6 February 2011
Accepted 8 February 2011
Available online 13 February 2011

Keywords:
NK_3 antagonist
Pyrazole
Antipsychotic

ABSTRACT

A series of 3-aryl-5-acylpiperazinyl-pyrazoles (e.g., **3a–b**) initially identified through a high-throughput screening campaign using the aequorin Ca^{2+} bioluminescence assay as novel, potent small molecule antagonists of the G protein-coupled human tachykinin NK_3 receptor (*h*NK3-R) is described. Preliminary profiling revealed poor plasma and metabolic stability for these structures in rodents. Further optimization efforts resulted in analogs with improved potency, stability, and pharmacokinetic properties as well as good brain permeability, for example, compounds **26** and **42**. Unexpected cytotoxicity was observed in such N-Me pyrazole structures as compounds **41–42**.

The NK_3 receptor (NK_3-R) is a GPCR that belongs to the tachykinin receptor family and is preferentially activated by neurokinin B (NKB).[1] NK_3-R is expressed centrally in cortical regions and in basal ganglia structures relevant to psychiatric disorders. Based on preclinical studies, NK_3-R has been found to modulate monoaminergic and GABA and glutamate neurotransmission in the mammalian brain, thus raising the speculation that NK_3-R modulators may be useful for treatment of psychological disorders such as schizophrenia.[2] Discovery of osanetant (**2**) by Sanofi researchers in 1994, and shortly thereafter, talnetant (**1a**) by GSK scientists fueled the search for non-peptidic antagonists to *h*NK_3-R[3] and has subsequently resulted in the development of many variants of such structures, especially in the case of talnetant.[4]

Compounds **3a–b** (Fig. 1) were two of the initial hit structures detected in our *h*NK_3-R high-throughput screening campaign, using the aequorin Ca^{2+} bioluminescence assay.[5] Of the two, the *ortho* anisyl analog **3b** was superior in potency and was further profiled. Thus **3b**, as an initial hit, was found to be reasonably potent in *h*NK_3-R binding (K_i = 1.1 μM) and in its cellular response in the aequorin assay (IC_{50} = 480 nM), even though it displayed a >10-fold right-shift in binding against *r*NK_3-R (*r*NK_3-R K_i = 12 μM). Furthermore, **3b** displayed a reasonable off-target selectivity profile, both in terms of *h*NK-R subtypes (*h*NK_1-R K_i = 6.7 μM, *h*NK_2-R K_i = 12 μM) as well as CYP P-450 isoforms (IC_{50} >15 μM for 3A4, 2D6, 1A2, 2C9, and 2C19). These considerations, together with the structural novelty of such structures as *h*NK_3 antagonists,[2–4] encouraged us to consider this series for further development. However preliminary profiling results quickly revealed additional challenges in terms of the instability of analogs **3a–b** in rodent plasma and hepatic microsomal stability assays (cf. Table 1), even though in human plasma and microsomal incubations these analogs proved significantly more stable (e.g., **3a** and **3b** human liver microsomes (HLM) $T_{1/2}$ = 55 and 71 min, respectively). In view of the practical utility of rat animal models in the development phase, we sought to evaluate whether such *h*NK_3-R antagonist structures were amenable to improvements in potency as well as the stability profiles.

The majority of the five-membered heterocyclic acids required for the present work were directly purchased. Conventional pyrazole synthesis through a 1,3-ketoester intermediate followed by cyclization with hydrazine (or ammonia for the pyrrole acid precursor[6] to **43**) and subsequent saponification of the ester afforded the pyrazole acid building blocks for analogs **22**, **24**, **27**, **29**, and **30**. The pyrazole sulfonyl chloride used to prepare analog **37** was made using an in situ diazotization approach as outlined in Scheme 1 (step f).[7] With the heterocyclic acid building blocks in hand, the preparation of arylpiperazines was carried out using Buchwald amination (step b, Scheme 2) for the phenylpiperazine analogs, or via reductive amination (Scheme 3) for analogs **5–9**. For structures with more elaborate *ortho*-alkoxy substituents (**20–21**), a benzyl group protective strategy was employed (Scheme 2). The syntheses were completed through amide coupling of the five-membered heterocyclic acids (step f, Scheme 2). Methyl-substituted piperazines (**38–40**) and pyrazole ring bioisostere variants (**41–45**) were also prepared as per Scheme 2. The versatility of

* Corresponding author.
E-mail address: hhoveyda@euroscreen.com (H.R. Hoveyda).

0960-894X/$ - see front matter © 2011 Elsevier Ltd. All rights reserved.
doi:10.1016/j.bmcl.2011.02.033

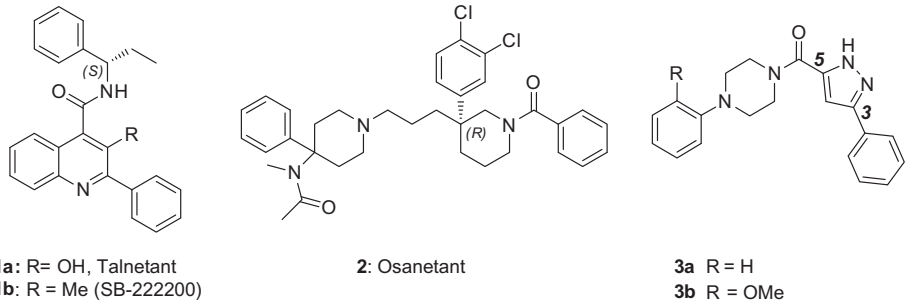

Figure 1. Structures of talnetant variants (**1a**–**b**), osanetant (**2**), and the initial hit structures (**3a**–**b**).

Table 1
Potency and stability SAR at Ring A

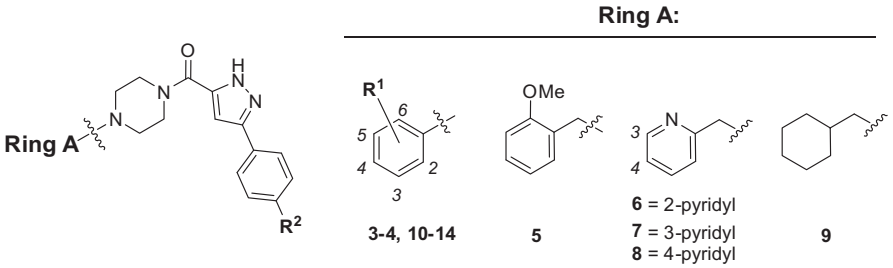

Compd	R^1	R^2	hNK$_3$ IC_{50}[a] (nM)	hNK$_3$ K_i[b] (nM)	RLM $T_{1/2}$ (min)	%Plasma stability[c]
3a	H	H	2100	ND[d]	9	15
3b	2-OMe	H	480	1100	5	3
4	2-OMe	Cl	130	250	3	8
5	See diagram	Cl	130	490	8	46
6	See diagram	Cl	5090	ND	ND	ND
7	See diagram	Cl	3810	ND	ND	ND
8	See diagram	Cl	1800	ND	ND	ND
9	See diagram	Cl	>10,000	ND	ND	ND
10	3-OMe	Cl	>10,000	ND	ND	ND
11	4-OMe	Cl	>10,000	ND	ND	ND
12	2-CF_3	Cl	>10,000	ND	ND	ND
13	2-CH_3	Cl	>10,000	ND	12	ND
14	2-Ph	H	>10,000	ND	ND	ND
15	2-Et	Cl	180	190	5	14
16	2-CN	Cl	480	ND	22	ND
17	2-OH	Cl	1300	ND	ND	ND
18	2-C(O)NH_2	Cl	>10,000	ND	ND	ND
19	2-OMe, 5-Cl	Cl	370	400	120	0
20	cf. Scheme 2	Cl	60	20	8	0
21	cf. Scheme 2	Cl	80	240	29	48

[a] Inhibition of NKB-induced aequorin Ca^{2+} signal in CHO cells expressing recombinant hNK$_3$-R.
[b] Displacement of [^{3}H]-labeled **1b** (cf. Fig 1) from recombinant hNK$_3$-R in CHO cells.
[c] Ex vivo rat plasma stability reported as % intact compound at 1 h.
[d] ND = no data.

reductive amination chemistry (Scheme 3) that includes ready access to myriad benzaldehyde building blocks was exploited using parallel synthesis to rapidly scan the potency SAR through benzylpiperazine (e.g., **5**) variants, with the most active analogs thus discovered confirmed subsequently in the corresponding phenylpiperazine (e.g., **4**) structure as well.

For brevity each of the four rings in the lead structure is annotated alphabetically (thus 'Rings A–D'), as defined in the illustrations that accompany Tables 1–4, and are used throughout the text.

In an early follow-up to the discovery of compound **3b** as an hNK$_3$-R antagonist hit, we observed that *para* chloro-substitution in Ring D (i.e., R^2 = Cl in **4**) further improved potency appreciably both in terms of binding and cellular response (cf. Table 1).[8] Moreover, **4** displayed a less right-shifted binding potency in rNK3-R (K_i = 250 nM) versus analog **3b** (K_i = 12 μM). Finally, analog **4** appeared to maintain the good off-target selectivity profile exhibited by **3b**, both in terms of hNK-R subtypes (hNK$_1$-R: K_i = 1.8 μM, hNK$_2$-R K_i = 8 μM) as well as CYP P-450 profile (IC_{50} >15 μM for 3A4, 2D6, 1A2, 2C9, and 2C19 isoforms). However, despite the overall improved in vitro bioactivity profile, **4** like **3b** proved unstable, especially in rat plasma and microsomal assays (cf. Table 1). Thus it remained to establish whether the instability issues observed in rodent assays in the more potent analog **4** could be improved. An additional early key observation was that *benzyl*piperazine analogs such as **5** were potent antagonists of hNK$_3$-R (cf. Table 1), but not of rNK$_3$-R (K_i = 4 μM). In terms of the initial off-target selectivity, **5** proved reasonably selective against hNK-R subtypes (hNK$_1$-R: K_i = 1.9 μM, hNK$_2$-R K_i = 19 μM), but it was less attractive than congener **4** in terms of its CYP P-450 profile with the IC_{50} values for three key isoforms 3A4, 2D6, and C9 determined as 8, 3, and 3 μM,

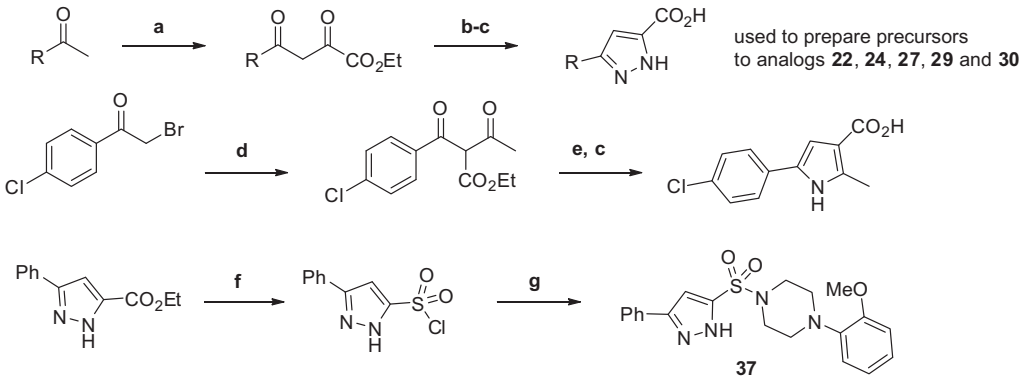

Scheme 1. Preparation of five-membered heterocyclic acids and sulfonyl chloride derivative. Reagents and conditions: (a) diethyloxalate, *t*-BuOK, toluene, rt, 8 h; (b) hydrazine, EtOH, reflux, 20 h; (c) NaOH, water/EtOH (1:1), reflux, 3 h; (d) ethyl acetoacetate, THF; (e) NH_3, acetic acid, 80 °C, 1 h; (f) concd HCl, 0 °C then $CuCl_2$, AcOH, SO_2 at rt; (g) *o*-anisyl-piperazine, DIEA, MeCN.

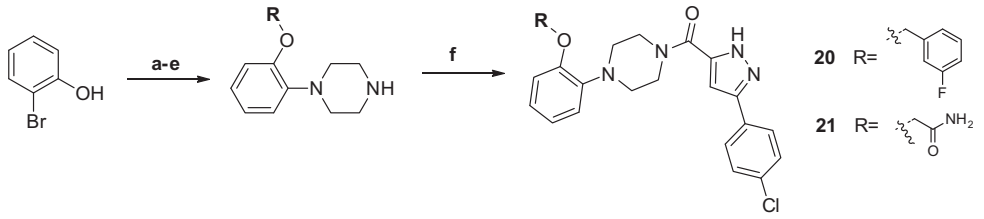

Scheme 2. Preparation of phenylpiperazine analogs. Reagents and conditions: (a) BnBr, K_2CO_3, 18-crown-6, MeCN, reflux, 20 h; (b) *N*-Boc-piperazine, X-Phos, $Pd(OAc)_2$, Cs_2CO_3, dioxane, reflux, 20 h; (c) 5% Pd/C, H_2, rt, 2 h; (d) 2-chloroacetamide or 1-(bromomethyl)-3-fluorobenzene, K_2CO_3, 18-crown-6, MeCN, reflux, 20 h; (e) 4 M HCl/dioxane, DCM, rt, 5 h; (f) pyrazole acid, HATU, NMM, DMF, 45 °C, 20 h.

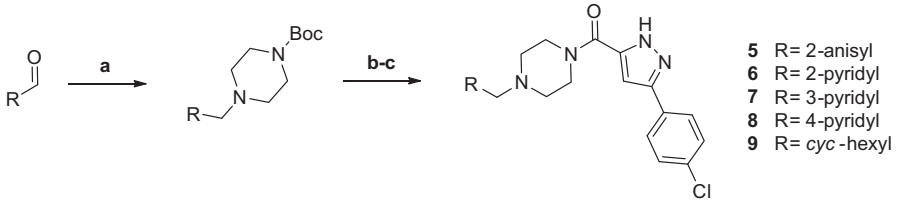

Scheme 3. Preparation of analogs **5**–**9**. Reagents and conditions: (a) $NaBH(OAc)_3$, *N*-Boc-piperazine, DCE/DCM, rt, 20 h; (b) 4 M HCl/dioxane, DCM, rt, 5 h; (c) phenyl-heterocycle-acid, HATU, NMM, DMF, 45 °C, 20 h.

respectively. Furthermore, **5** offered no advantages in terms of rat plasma stability versus **4** and also displayed a short half-life of 8 min in the rat liver microsome assay (cf. Table 1). Thus a greater preference was accorded to the phenylpiperazine analogs, exemplified by **4**, which also contain one less rotatable bond than **5**,[9] whereas the benzylpiperazine variants[10] were utilized for a rapid initial scan of the potency SAR through generation of focused libraries.

Reduction of the aryl ring to cyclohexyl at Ring A resulted in an inactive structure (e.g., **9** vs **5**, Table 1), while reduction of Ring D caused a significant (⩾fourfold) right shift in potency (e.g., **35** vs **3b**, Tables 1 and 2), indicating a preference for an aromatic Rings A–D combination for good *h*NK_3-R antagonist potency. Contrary to the phenyl ring structures, pyridyl ring variants failed to furnish potent antagonists when applied either at Ring A (**6–8** vs **5**, Table 1) or at Ring D (**32**–**34** vs **4**, Tables 1 and 2). However, exploration of the impact of aromatic ring substitution in Rings A and D in terms of *h*NK_3-R antagonist potency SAR proved more fruitful. As mentioned above, *ortho* anisyl Ring A had a significant (∼fourfold) impact on potency as revealed by a comparison of IC_{50} values for **3a** versus **3b** (cf. Table 1). Indeed *ortho* substitution in Ring A was typically preferred over *meta* or *para* analogs as exemplified by the three anisyl Ring A regioisomers (**4**, **10**–**11**). In terms of the nature of *ortho* substituents, the potency SAR results did not correlate either with the electronic or the lipophilicity properties of the substituent. For example, both *ortho* methyl and *ortho* CF_3 moieties resulted in inactive compounds (**12**, **13**), yet both *ortho* cyano (**16**) and *ortho* ethyl (**15**) Ring A analogs yielded comparatively active antagonists (cf. Table 1). Comparison between *ortho* phenol (**17**) versus *ortho* anisyl (**4**) congeners and between *ortho* methyl versus ethyl analogs (**13** vs **15**) seemed to suggest that for optimal receptor interaction, the *ortho* Ring A side-chain must be comprised of two heavy (non-hydrogen) atoms. Subsequently, the latter structural feature was further investigated using a wide range of *ortho* Ring A substituents bearing a rotatable bond (comprised of two non-hydrogen atoms), initially through the benzylpiperazine variants, as discussed above. The most active analogs were eventually confirmed in the analogous phenylpiperazine structures, such as with **20**–**21**, *h*NK_3-R IC_{50} <90 nM (Table 1). The significant impact of the presence of a rotatable bond linker at the *ortho* substituent in Ring A in terms of antagonist potency was again apparent by comparing analogs **20** versus **14** and **21** versus **18**. In each case the absence of a rotatable bond resulted in an inactive analog (**14**, **18**: IC_{50} >10 μM), in sharp contrast to the po-

Table 2
Potency and stability SAR at Ring D

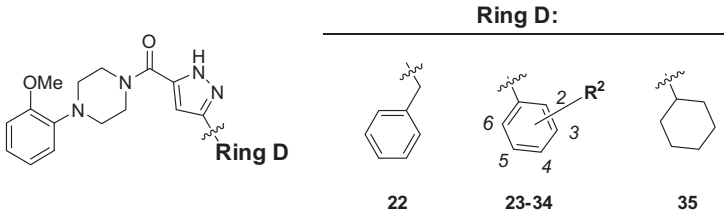

Compd	R^2	hNK_3 IC_{50} (nM)	hNK_3 K_i (nM)	RLM $T_{1/2}$ (min)	%Plasma stability
22	See diagram	3300	ND	ND	ND
23	2-F	1200	2500	ND	ND
24	3-F	580	1600	ND	ND
25	4-F	240	530	4	18
26	4-CF_3	42	120	5	55
27	4-OCF_3	130	310	5	59
28	4-CH_3	390	510	ND	ND
29	4-SO_2Me	2500	ND	ND	ND
30	4-CN	208	700	8	91
31	2,4-DiCl	205	260	45	5
32	2-N	3100	3600	ND	ND
33	3-N	7100	ND	ND	ND
34	4-N	7200	ND	ND	ND
35	See diagram	2000	2900	ND	ND

Table 3
Potency and stability SAR at Ring B

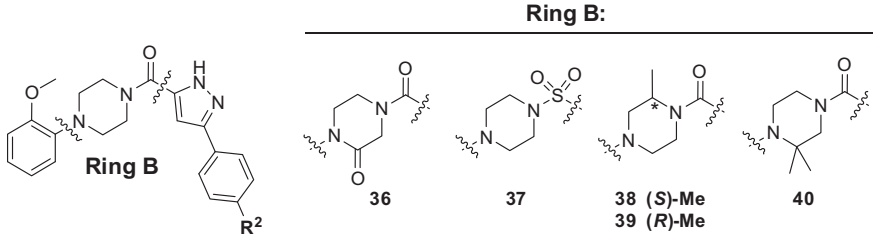

Compd	R^2	hNK_3 IC_{50} (nM)	hNK_3 K_i (nM)	RLM $T_{1/2}$ (min)	%Plasma stability
36	Cl	3100	ND	ND	ND
37	H	7400	ND	ND	ND
38	Cl	190	370	2	100
39	Cl	2900	ND	ND	ND
40	Cl	93	240	147	48

tent analogs bearing similar side-chains but attached through a rotatable bond linker (**20–21**: IC_{50} <90 nM). In addition to improved potency, the ca. tenfold improved rodent metabolic stability in analog **21** ($c\log P = 2.8$) versus **4** ($c\log P = 4.4$)[11] is consistent with the reduced lipophilicity in **21** through introduction of the polar acetamide side-chain. In addition, we observed that metabolic blocking through chloro-substitution in Ring A *para* to the electron-rich *ortho* anisyl moiety also imparted significant metabolic stability to the attendant molecule (cf. **19** RLM $T_{1/2}$ = 120 min in Table 1), although the rodent plasma instability issue remained unaffected. Overall, these results demonstrated the utility of Ring A to improve potency and rodent metabolic stability through either reduction of lipophilicity and/or through metabolic blocking strategies.

In terms of monosubstituted Ring D analogs, *para* substitution was typically optimal for antagonist potency, as exemplified through fluoro-substituted congeners (**23**–**25**, Table 2). In stark contrast with Ring A, for Ring D a clear SAR was observed in that the most potent analogs appeared to be confined to those possessing lipophilic and electron-withdrawing substituents. For example, *para*-CF_3 analog **26** (IC_{50} = 42 nM) was nearly tenfold more potent than the *para* toluyl congener (**28**, Table 2). Likewise, *para*-OCF_3 analog **27** proved significantly more potent than **29**–**30** that bear polar electron-withdrawing substituents (thus not lipophilic). Interestingly, analogs **26**–**27** and **30** with *para* electron-withdrawing substituents in Ring D displayed improved ex vivo plasma stability but not microsomal metabolic stability in rats. Moreover, further reduction of electron density in phenyl Ring D through dichloro-substitution at both *ortho* and *para* phenyl ring positions (**31**, Table 2) resulted in significant improvement in rat microsomal half-life, albeit with little impact either on rodent plasma stability, or on hNK_3-R antagonist potency (vs **4**). Thus collectively, the foregoing results on aryl Rings A and D demonstrate that substitution on these aromatic rings plays an important role in modulation of potency and stability profiles.

Concerning the SAR for the piperazine ring (Ring B) and the associated amide bond, the following serve as the key highlights (cf. Table 3). Analog **36**, wherein the piperazine ring was replaced with a ketopiperazine ring, proved to be ~24 times less potent than **5**; this established the importance of the sp^3 hybridized basic

Table 4
Potency and stability SAR at Ring C

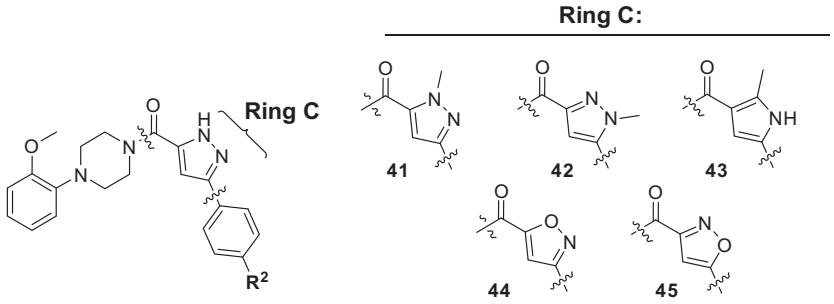

Compd	R^2	*h*NK$_3$ IC_{50} (nM)	*h*NK$_3$ K_i (nM)	RLM $T_{1/2}$ (min)	%Plasma stability
41	Cl	180	540	44	100
42	Cl	180	370	40	100
43	Cl	280	350	17	100
44	H	>5000	ND	ND	ND
45	Cl	1100	1800	17	78

Table 5
Comparative evaluation of the in vitro and in vivo profiles of analogs **1a**, **2** versus **41**–**42**

	1a	**2**	**41**	**42**
Subtype selectivity, K_i[a] (nM)				
*r*NK$_3$	190	57	3700	3400
*h*NK$_3$	7.4	1.9	540	370
*h*NK$_2$	3700	85	10,000	13,000
*h*NK$_1$	>10,000	330	2200	1600
CYP P-450, IC_{50} (μM)				
3A4, 2D6, 1A2	4, 18, 5	1, 55, >100	12, 29, 21	20, 42, 34
2C9, 2C19	2, 9	11, 7	3, 6	4, 9
% Cell viability (HepG2)[b]	82%	97%	6.7%	8.5%
Stability and protein binding (rat)				
RLM, $T_{1/2}$ (min)	60	23	44	40
Plasma stability (at 60 min)	100%	NA	100%	100%
% Plasma protein binding	99.9	99.4	99.5	99.8
Pharmacokinetics (rat)[c]				
CL (mL/min/kg)	1.9	57	13	7.3
V_{dss} (L/kg)	1.4	8.7	4.9	3.3
$T_{1/2}$ (min)	450	110	270	310
AUC oral dosing (ng min/mL)	933,806	6856	ND	90,501
%F	53	17	NA	53
Brain penetration (mouse)[d]				
Brain:plasma ratio (at 10 min)	0.07	0.03	0.88	0.64
Brain concn (ng/g) at 10 min	340	30	830	1700

[a] Radioligand binding assay.
[b] Measured at 50 μM test concentration after 24 h.
[c] Male Sprague–Dawley rats at 1 mg/kg iv and 3 mg/kg po in physiological saline with 9% 2-hydroxypropyl-β-cyclodextrin (HP-β-CD).
[d] Male CD-1 mice at 5 mg/kg ip in physiological saline with 9% HP-β-CD.

nitrogen in piperazine for optimal receptor interactions. Replacing the piperazine amide juncture with sulfonamide (**37**) resulted in ~15-fold right shift in potency (vs **3b**, Table 1). Moreover, methyl substitution on the piperazinyl ring provided further noteworthy results summarized below. Thus methyl substitution at the carbon adjacent to the amide piperazine nitrogen displayed a stereospecific potency SAR with the (*S*)-Me enantiomer (**38**, Table 3) proving to be ~15-fold more potent than its antipode (**39**) and nearly equipotent to the reference analog **4** (Table 1). Importantly, analog **38** was found to be fully stable in rat plasma contrary to **4** that was rather unstable in rat plasma. Nonetheless, the rat microsomal stability remained comparable between the latter analogs (RLM $T_{1/2}$ 2–3 min). The improved rat plasma stability in **38** may stem from steric occlusion of the potentially hydrolyzable amide linkage.[12] Interestingly, analog **40** (RLM $T_{1/2}$ = 147 min) proved more robust than congener **38** in terms of rat microsomal stability whereas its rat plasma stability profile, while significantly better than **4**, was inferior to **38**. Analog **40** was not pursued further due to inferior plasma stability; nonetheless, these results made abundantly clear that the piperazine ring modifications provide yet another avenue for advanced lead optimization in the foregoing *h*NK$_3$-R antagonist series.

Principle features of the SAR for the five-membered heteroaryl ring segment in the current lead structures are summarized in Table 4. Replacing the pyrazole ring with an isoxazole ring resulted in ⩾eightfold loss of potency irrespective of the regioisomerism (cf. **44** vs **3b** and **45** vs **4**). Yet the 2-methyl-pyrrole bioisostere (**43**) was merely twofold right-shifted in potency (vs **4**, Table 1). Moreover, analog **43** proved devoid of rat plasma stability issues and displayed moderately improved rat microsomal half-life of

17 min. The results for analog **43**, together with the relatively good hNK$_3$-R antagonist potency in the *N*-methyl pyrazole regioisomers, **41–42**, tend to suggest that the diminished potency in isoxazole isosteres is unrelated to the absence of the hydrogen bond donor present in an unsubstituted pyrazole ring such as **4**. In fact, the best analogs in terms of the overall potency and stability profiles turned out to be the *N*-methyl pyrazole analogs, **41–42**. The improved plasma stability in *N*-methyl pyrazole analog **41** recalls the effect of methyl piperazine substitution in **38** that was suggested to be at least partially due to steric occlusion nearby the amide linker (vide supra). While the hNK$_3$-R antagonist potency in the latter analogs only marginally differed from the reference analog **4**, the rat plasma and microsomal stability profiles in **41** and **42** were significantly ameliorated. Thus both analogs proved to be completely stable in rat plasma in addition to displaying $T_{1/2}$ >40 min in the rat microsomal assay.

A comparative evaluation of analogs **41**–**42** against talnetant (**1a**) and osanetant (**2**) is provided in Table 5.[13] Among all analogs, a right shift was observed in terms of human versus rodent NK$_3$-R binding potency, with talnetant showing >25-fold shift vis-à-vis ~30-fold shift for osanetant and ~10-fold shift for **41**–**42**. In addition, for all four analogs the best NK-subtype selectivity is that of hNK$_3$:hNK$_2$ with talnetant being the most selective (500-fold), while osanetant and analogs **41**–**42** display a ~20- to 50-fold selectivity. In terms of hNK$_3$:hNK$_1$ selectivity the following trend is discernible: talnetant (>1000-fold) > osanetant (174-fold) > **41**–**42** (4- to 7-fold). However, in terms of CYP P-450 profile, analogs **41**–**42** proved superior to talnetant or osanetant. In addition, **41** and **42** were cleared from systemic circulation in rats at a reasonably low rate, 3- to 6-fold more rapidly than talnetant[14] and significantly superior to the essentially flow-limited clearance rate for osanetant. Compounds **41**–**42** also displayed distribution volumes 5- to 10-fold that of total body water, and were present at 0.5% and 0.2% fraction unbound based on plasma protein binding data in rats. Analog **42** was also found to be 53% orally bioavailable in rat. Indeed both **41** and **42** were found to be highly CNS-penetrant, superior in this respect to both talnetant and osanetant, both in relative (brain-to-plasma ratios >0.6) and in absolute terms (>800 ng/g at 10 min). Overall these analogs displayed promising pharmacokinetic and brain permeability profiles in rodents and as such appear to be viable entities for further lead development towards CNS therapeutic agents.

Despite these promising developments, however, high levels of cytotoxicity (assessed in HepG2 cells at 50 μM after 24 h) were encountered in **41** and **42** (cf. Table 5). These results were somewhat unexpected given the absence of any significant cytotoxicity in several non-methylated pyrazole analogs such as **4**, and clean toxicology profile reported on related structures in the literature.[15] Nonetheless, these results tend to implicate a potential role for N-Me pyrazole as a toxicophore in such structures as **41**–**42**.

We described herein a series of novel hNK$_3$ antagonists that proved amenable to optimization in terms of hNK$_3$-R antagonist potency and rodent stability profiles through several types of structural modifications. Structures with good potency and oral bioavailability that were CNS-penetrant were achievable in this series, as exemplified by analog **42**. Ultimately this work was abandoned in view of the cytotoxicity issue encountered in a subset of these structures (namely **41** and **42**) and further prompted by discovery of other more promising lead series in this program, which will be reported in due course.

Acknowledgment

We are grateful to Dr. Vladimir Trukhan and his team at the ChemBridge Corporation, Moscow, Russia, for executing the synthetic chemistry in support of this project.

References and notes

1. Spooren, W.; Riemer, C.; Meltzer, H. *Nat. Rev. Drug Disc.* **2005**, *4*, 967.
2. Smith, P. W.; Dawson, L. A. *Recent Patents CNS Drug Disc.* **2008**, *3*, 1.
3. Giardina, G. A. M.; Raveglia, L. F. *Expert Opin. Ther. Patents* **1997**, *7*, 307.
4. See for example: (a) Smith, P. W.; Wyman, P. A.; Lovell, P.; Goodacre, C.; Serafinokwska, H. T.; Vong, A.; Harrington, F.; Flynn, S.; Bradley, D. M.; Porter, R.; Coggon, S.; Murkitt, G.; Searle, K.; Thomas, D. R.; Watson, J. M.; Martin, W.; Wu, Z.; Dawson, L. *Bioorg. Med. Chem. Lett.* **2009**, *19*, 837; (b) Elliott, J. M.; Carling, R. W.; Chambers, M.; Chicchi, G. G.; Hutson, P. H.; Jones, A. B.; MacLeod, A.; Marwood, R.; Mensese-Lorente, G.; Mezzogori, E.; Murray, F.; Rigby, M.; Royo, I.; Russell, M. G. N.; Sohal, B.; Tsao, K. L.; Williams, B. *Bioorg. Med. Chem. Lett.* **2006**, *16*, 5748; (c) Xiong, H.; Kang, J.; Woods, J. M.; McCauley, J. P., Jr.; Koether, G. M.; Albert, J. S.; Hinkley, L.; Gadient, R. A.; Simpson, T. R. *Bioorg. Med. Chem. Lett.* **2010**. doi:10.1016/j.bmcl.2010.11.003.
5. Le Poul, E.; Hisada, S.; Mizuguchi, Y.; Dupriez, V. J.; Burgeon, E.; Detheux, M. *J. Biomol. Screen.* **2002**, *7*, 57. Euroscreen has developed stably transfected cell lines with plasmids encoding apoaequorin, the GPCR of interest (e.g., hNK$_3$-R), and, if needed, a recombinant G-protein to redirect receptor coupling towards Ca^{2+} signaling. Upon receptor activation, the change in intracellular [Ca^{2+}] causes a conformational change in the aequorin protein thereby eliciting a quantifiable luminescent signal. This method is adapted to detect agonist, antagonist or allosteric modulators of receptor activity.
6. Petruso, S.; Caronna, S.; Sferlazzo, M.; Sprio, V. *J. Heterocycl. Chem.* **1990**, *27*, 1277.
7. Bellemin, R.; Festal, D. *J. Heterocycl. Chem.* **1984**, *21*, 1017.
8. Given the good agreement between the radioligand binding and aequorin functional assays, the latter set of results will be principally used in foregoing SAR discussions.
9. Veber, D. F.; Johnson, S. R.; Cheng, H. Y.; Smith, B. R.; Ward, K. W.; Kopple, K. D. *J. Med. Chem.* **2002**, *45*, 2615.
10. No appreciable solubility difference between **4** and **5** was detectable at pH 7, although at pH 5 benzylpiperazine analog **5** was decidedly more soluble.
11. *C* log *P* values cited herein are calculated using ChemBioDraw (CambridgeSoft, v.12).
12. Kerns, E. H.; Di, L. *Drug-like Properties: Concepts, Structure Design and Methods: From ADME to Toxicity Optimization*; Academic Press: Burlington, Massachusetts, 2008. Chapter 12.
13. Talnetant was made and characterized as per: (a) Giardina, G. A. M.; Sarau, H. M.; Farina, C.; Medhurst, A. D.; Grugni, M.; Foley, J. J.; Raveglia, L. F.; Schmidt, D. B.; Rigolio, R.; Vassallo, M.; Vecchietti, V.; Hay, D. W. P. *J. Med. Chem.* **1996**, *39*, 2281; Osanetant was purchased from Charnwood Molecular, UK. It was made and characterized as per: (b) Giardina, G. A. M.; Grugni, M.; Rigolio, R.; Vassllo, M.; Erhard, K.; Farina, C. *Bioorg. Med. Chem. Lett.* **1996**, *6*, 2307; (c) Chen, H. G.; Chung, F.-Z.; Goel, O. P.; Kesten, J. S.; Knobelsdorf, J.; Lee, H. T.; Rubin, J. R. *Bioorg. Med. Chem. Lett.* **1997**, *7*, 555.
14. For a report on the pharmacokinetic profile of talnetant, see Tables 2 and 3 in: Sarau, H. M.; Griswold, D. E.; Potts, W.; Foley, J. J.; Schmidt, D. B.; Webb, E. F.; Martin, L. D.; Brawner, M. E.; Elshourbagy, N. A.; Medhurst, A. M.; Giardina, G. A. M.; Hay, D. W. P. *J. Pharmacol. Exp. Ther.* **1997**, *281*, 1303. The reported values in Table 5 herein are in agreement with those in the cited reference.
15. For example: Martres, P.; Faucher, N.; Laroze, A.; Pineau, O.; Fouchet, M.-H.; Potvain, F.; Grillot, D.; Beneton, V. *Bioorg. Med. Chem. Lett.* **2008**, *18*, 6251. Compound **7** (GSK183390A) in the cited reference is depicted below and has been reported to have a clean 7-day toxicology profile in rats with no safety issues.

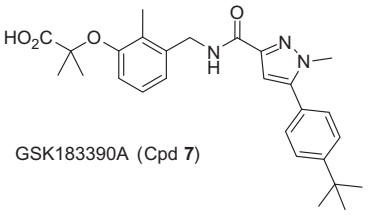

GSK183390A (Cpd **7**)